

We are IntechOpen, the world's leading publisher of Open Access books Built by scientists, for scientists

6,900

Open access books available

186,000

International authors and editors

200M

Downloads

Our authors are among the

154

Countries delivered to

TOP 1%

most cited scientists

12.2%

Contributors from top 500 universities



WEB OF SCIENCE™

Selection of our books indexed in the Book Citation Index
in Web of Science™ Core Collection (BKCI)

Interested in publishing with us?
Contact book.department@intechopen.com

Numbers displayed above are based on latest data collected.
For more information visit www.intechopen.com



Mass Transfer in Fluidized Bed Drying of Moist Particulate

Yassir T. Makkawi¹ and Raffaella Ocone²

¹Chemical Engineering & Applied Chemistry, Aston University, Birmingham B4 7ET,

²Chemical Engineering, Heriot-Watt University, Edinburgh EH14 4AS,
UK

1. Introduction

Bubbling fluidized bed technology is one of the most effective means for the interaction between solid and gas flow, mainly due to its good mixing and high heat and mass transfer rate. It has been widely used at a commercial scale for drying of grains such as in pharmaceutical, fertilizers and food industries. When applied to drying of non-porous moist solid particles, the water is drawn-off driven by the difference in water concentration between the solid phase and the fluidizing gas. In most cases, the fluidizing gas or drying agent is air. Despite of the simplicity of its operation, the design of a bubbling fluidized bed dryer requires an understanding of the combined complexity in hydrodynamics and the mass transfer mechanism. On the other hand, reliable mass transfer coefficient equations are also required to satisfy the growing interest in mathematical modelling and simulation, for accurate prediction of the process kinetics.

This chapter presents an overview of the various mechanisms contributing to particulate drying in a bubbling fluidized bed and the mass transfer coefficient corresponding to each mechanism. In addition, a case study on measuring the overall mass transfer coefficient is discussed. These measurements are then used for the validation of mass transfer coefficient correlations and for assessing the various assumptions used in developing these correlations.

2. Two phase model of fluidization

The first model to describe the essential hydrodynamic features in a bubbling fluidized bed, usually referred to as the simple two phase model, was proposed in the early fifties of the last century by Toomey and Johnstone (1952). The model assumes that all the gas in excess of the minimum fluidization velocity, U_{mf} , passes through the core of the bed in the form of bubbles. The rest of the gas, usually referred to as emulsion gas, was described to pass through a dense solid phase surrounding the bubbles, at a low velocity close or equal to U_{mf} . Later experimental investigations on bubbles formation and rise in two and three dimensional fluidized beds, utilizing conventional photographing and x-ray imaging techniques, have shown a rather more complicated flow pattern of gas around bubbles. A more accurate model, describing the movement of gas/solid and pressure distribution

around a rising bubble was then proposed by Davidson and Harrison (1963). This model describes the gas flow through a three dimensional fluidized bed mainly in a spherical or semi-spherical shape bubbles through the core, however, depending on the emulsion gas velocity; the region around the bubble may be surrounded by a cloud as a result of emulsion gas circulation between the dense solid phase and the core of the bubble. This can be schematically described as shown in Fig. 1. The existence of a cloud around fast rising bubbles has been later verified experimentally by a number of researchers. Most recently, Makkawi and Ocone (2009), utilizing Electrical Capacitance Tomography (ECT) imaging have further confirmed the existence of cloud around a single isolated bubble rising through a fluidized bed as shown in Fig. 2. In terms of mass transfer, the existence of cloud and gas circulation between the bubble and its surrounding have a significant contribution to the overall mass transfer mechanism in a bubbling fluidized bed dryer as will be discussed later.

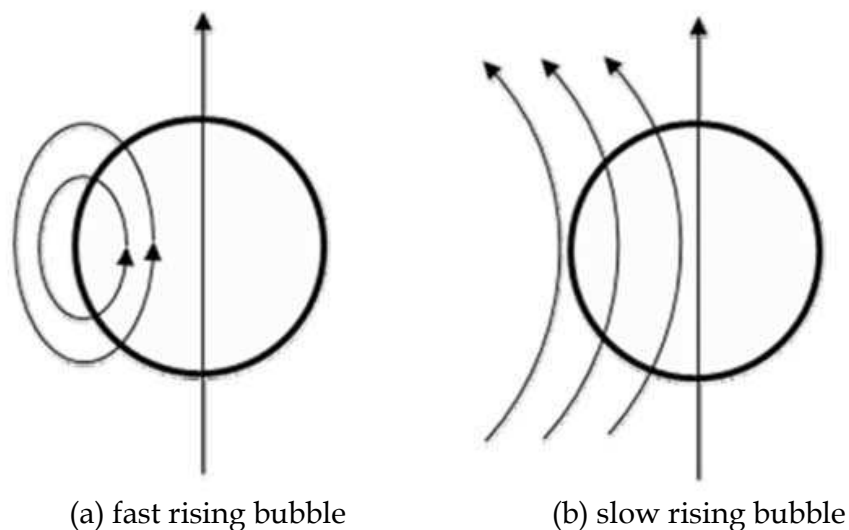


Fig. 1. Proposed gas streamlines in and out of a single rising bubble as described in

3. Mass transfer mechanisms

With the confirmed existence of different phases in a bubbling fluidized bed, it is postulated that in a bubbling fluidized bed dryers different mechanisms can regulate the mass transfer process, depending on the bubbles characteristics and the degree of water content in the bed. The different phases, which all contribute to the removal of moisture from the wet particles, are the bubble phase, its surrounding cloud and the dense annular solid phase.

The most widely used mass transfer model of Kunii and Levenspiel (1991) expresses the overall mass transfer in a bubbling bed in terms of the cloud-bubble interchange and dense-cloud interchange. The cloud-bubble interchange is assumed to arise from the contribution of circulating gas from the cloud phase and in and out of the bubble, usually referred to as throughflow, in addition to the diffusion from a thin cloud layer into the bubble. The dense-cloud interchange is assumed to arise only from diffusion between the dense phase and the cloud boundary. Kunii and Levenspiel (1991) also suggested additional mass transfer resulting from particles dispersed in the bubbles, however, recent advanced imaging technique, have shown bubble free particles in most cases as will be demonstrated later.

For particles of about 500 μm , some researchers assume that the transfer is of a purely diffusional nature, and thus neglect the contribution of bubble throughflow. However, Walker [1975] and Sit and Grace [1978] pointed out that, pure diffusional model may significantly underestimate, the overall mass transfer coefficient. Kunii and Levenspiel (1991) reported that the true overall mass transfer coefficient may fall closer to either of the acting mechanisms depending on the operating conditions (particle size, gas velocity, etc.). They suggested accounting for the first mechanism by summing the diffusional and throughflow, and adding those to the second mechanism in a similar fashion as for additive resistances.

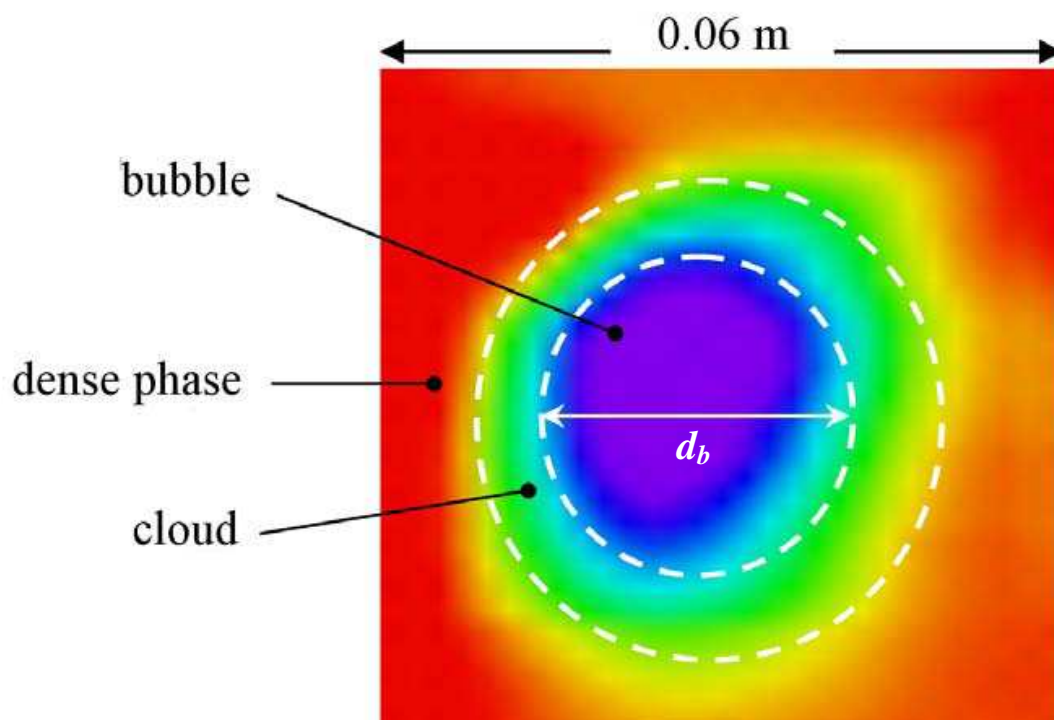


Fig. 2. Dense-cloud and cloud-bubble phases demonstrated in a typical ECT image of an isolated rising clouded bubble in a fluidized bed

4. Mass transfer coefficient from literature

Because of the growing interest on modelling as a tool for effective research and design, researchers on bubbling fluidized bed drying or mass transfer in general are nowadays seeking to validate or develop new mass transfer coefficient equations required for accurate prediction of the process kinetics. Recently, different mass transfer coefficients for drying in fluidized beds have been reported in the literature, most of them are based on the two phase model of fluidization.

Ciesielczyk and Iwanowski (2006) presented a semi-empirical fluidized bed drying model based on cloud-bubble interphase mass transfer coefficient. To predict the generalized drying curve for the solid particles, the interchange coefficient across the cloud-bubble boundary was given by:

$$K_{cb} = 4.5 \left(\frac{u_{mf}}{d_b} \right) + 5.85 \left(\frac{g^{0.5} g^{0.25}}{d_b^{1.25}} \right) \quad (1)$$

where the bubble diameter, d_b , is given by modified Mori and Wen (1975) model for the bubble diameter as follows:

$$\frac{d_{b,m} - d_b}{d_{b,m} - d_{b,0}} = \exp\left(-\frac{0.12H_{mf}}{D_c}\right) \quad (2)$$

where $d_{b,0}$ and $d_{b,m}$ are the initial bubble diameter at the distributor level and at its maximum size respectively, and given by:

$$d_{b,0} = 0.376(U - U_{mf})^2 \quad (3)$$

$$d_{b,m} = 1.636\left[D_c(U - U_{mf})\right]^{0.4} \quad (4)$$

According to Davidson and Harrison (1963), the first term in the right side of Eq. 1 is assumed to represent the convection contribution as a result of bubble throughflow. The second term arises from the diffusion across a limited thin layer where the mass transfer takes place. Using area based analysis, Murray (1965) suggested that the first term on the right side of Eq. 1 to be reduced by a factor of 3, which then gives:

$$K_{cb} = 1.5\left(\frac{u_{mf}}{d_b}\right) + 5.85\left(\frac{\mathcal{D}^{0.5}g^{0.25}}{d_b^{1.25}}\right) \quad (5)$$

Ciesielczyk and Iwanowski (2006) have shown satisfactory agreement between the above outlined correlation and experimentally determined drying rate and mass transfer coefficient for group B particles of Geldart classification.

Kerkhof (2000) discussed some modeling aspect of batch fluidized bed drying during thermal degradation of life-science products. In this model, it is assumed that the contribution from particle raining or circulating in and out from a bubble is important, therefore the cloud-bubble interphase exchange, given by Eq. 1 above, was combined with the dense-cloud exchange in addition to contribution from the particle internal diffusion to give an overall bed mass transfer coefficients,

$$Sh_{bed} = Sh_{pb} + Sh_{db} \quad (6)$$

where the first sherwood number, Sh_{pb} , represents the mass transfer added from the particles dispersed in the bubble and expressed in terms of the mass transfer coefficient for a single particle, given by,

$$k_{pb} = \frac{\mathcal{D}}{d_p}\left(2 + 0.664Re_p^{0.5}Sc^{0.33}\right) \quad (7)$$

The second Sherwood number, Sh_{db} , represents the combined cloud-bubble and dense-cloud exchanges and given in terms of a single mass transfer coefficient, k_{db} , as follows,

$$\frac{1}{k_{db}} = \frac{1}{k_{dc}} + \frac{1}{k_{cb}} \quad (8)$$

where the cloud-bubble mass transfer coefficient, k_{cb} , was given earlier in Eq. 1 in terms of interchange coefficient. Note that the interchange coefficient is expressed as a rate constant (1/s), which can then be multiplied by the bubble volume per unit area to give the mass transfer coefficient in (m/s) as follows:

$$k = \frac{d_b}{6} K \quad (9)$$

The dense-cloud mass transfer coefficient, k_{dc} , which appear in Eq. 8 was adopted from Higbie penetration model, which is expressed in terms of the bubble-cloud exposure time and the effective diffusivity as follows:

$$k_{dc} = 2 \left(\frac{\mathcal{D}_e \varepsilon_{mf}}{\pi t} \right)^{0.5} \quad (10)$$

where $t = \frac{d_c}{u_b}$ is the exposure time between the bubble and the cloud. Kerkhof (2000) made

two simplifications to Eq. 10; first, it is assumed that the cloud thickness is negligible, therefore the bubble diameter can be replacement for the cloud diameter (i.e. $d_c \approx d_b$), second, it is assumed that the effective diffusivity is better approximated by the gas molecular diffusivity (i.e. $\mathcal{D}_e \approx \mathcal{D}$). Accordingly, Eq. 10 reduces to

$$k_{dc} = 6.77 \left(\frac{\mathcal{D} \varepsilon_{mf} u_b}{d_b^3} \right)^{0.5} \quad (11)$$

Recently, Scala (2007) experimentally studied the mass transfer around a freely active particle in a dense fluidized bed of inert particles. The results suggested that the mass transfer coefficient for a single particle is best correlated by a modified Foessling (1938) equation for Sherwood number,

$$Sh = 2\varepsilon_{mf} + 0.7 \text{Re}_{p,mf}^{0.5} \text{Sc}^{0.33} \quad (12)$$

where $\text{Re}_{p,mf}$ is the Reynolds number expressed in terms of the voidage ε_{mf} (i.e. $= \rho u_{mf} d_p / \mu \varepsilon_{mf}$). The above correlation was found to be independent of the fluidization velocity or regime change from bubbling to slugging. Accordingly, Scala (2007) concluded that in a dense bubbling bed the active particle only reside in the dense phase and never enters the bubble phase, hence it has no direct contribution to the bubble-dense phase interchanges. This contradicts the observation noted by Kunii and Levenspiel (1991) and others (e.g. Kerkhof, 2000; Agarwal, 1978), were it is assumed that the contribution of particles dispersed in the bubble should not be neglected. Agarwal (1978) claimed that the particles do circulate in and out of the bubble with 20% of the time residing within the bubble phase.

Clearly, despite of the considerable effort on developing fluidized bed mass transfer coefficients, there still remain uncertainties with respect to the assumptions used in developing these coefficients.

5. Characteristic drying rate profiles

Early experimental observations on fluidized beds suggest that the mass transfer at the single particle level generally occurs at two different drying regimes; one at which the free moisture, either at the particle surface or within large pores, is rapidly withdrawn at a constant rate, followed by a slower rate regime at which the process is controlled by slow diffusion from the fine pores to the particle surface. These are usually referred to as “constant rate” and “falling rate” respectively. The moisture content at the transition between these two regimes is called the critical moisture content. Fig. 3 illustrates the characteristic drying rate curve as function of time and moisture content. There is an argument that these drying curves are in fact oversimplification of the process, and such profiles may change considerably with respect to particle size and material type. Keey (1978) pointed that the drying rate at the beginning of the process may not be constant at all, or at least changes to a small degree, therefore, he recommended calling this as “initial drying period” instead of the commonly used term “constant drying”. The same applies to the “falling rate” regime, where it is preferred to call it “second drying period”. The existence of the critical moisture content point, on the other hand, is true in most cases.

For non-pours particles, regardless of the material type, the drying process occurs at a single regime, where the moisture residing at the particle surface is rapidly withdrawn, driven by difference in moisture concentration. To a great extent, this resembles free water diffusion into a moving air stream. Fig. 4 shows an example of this behaviour during drying of wet glass beads in a bubbling fluidized bed using air at ambient conditions.

Here it is clear that the drying rate falls exponentially within the first 15 minutes, after which the drying process ends. This confirms a single drying regime rapidly driven by the difference in moisture content between the fluidizing air and particle. Using the data in Fig. 4, one can obtain the water concentration in the fluidized bed as a function of the drying time by the integration of the drying curve function, $F(t)$, such that

$$w_t = w_o - \int_0^t F(t) dt \quad (13)$$

where w_o is the initial water content.

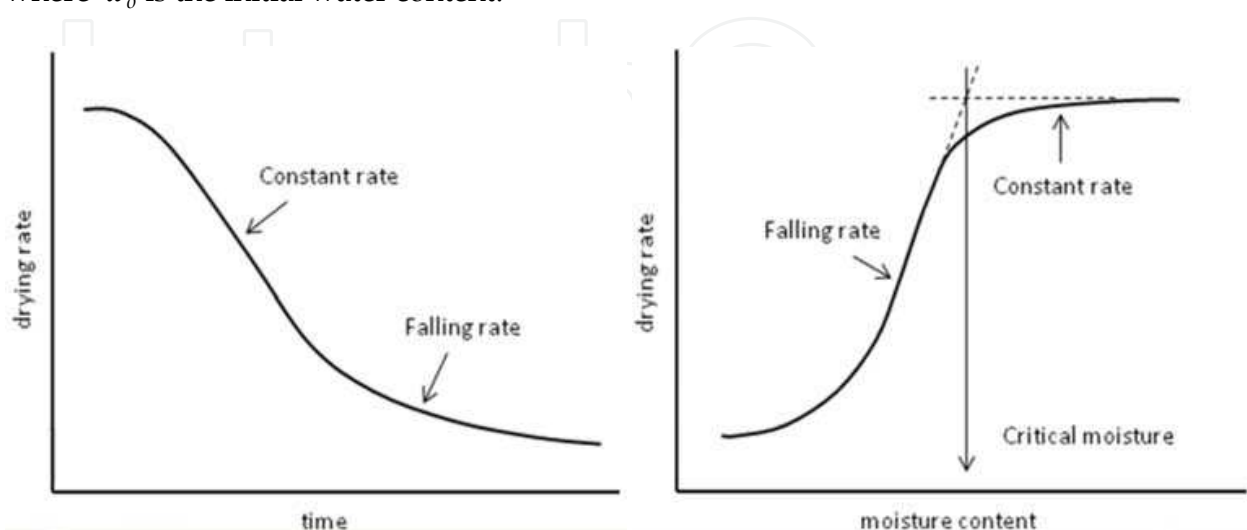


Fig. 3. Characteristic drying curves for moist particles

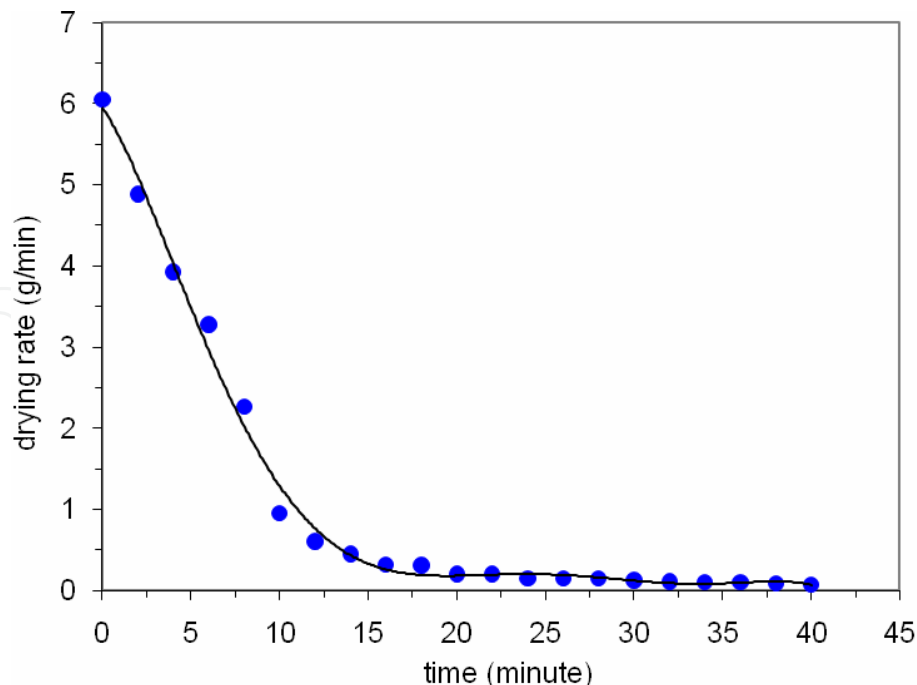


Fig. 4. Drying rate profile for moist glass beads in a bubbling fluidized bed using ambient air (Makkawi and Ocone, 2009).

6. Case study

Experiments have been carried out with the primary objective to measure the mass transfer coefficient for a drying process in a conventional bubbling fluidized bed. This required detailed knowledge of the fluidized bed hydrodynamics and drying rate. For this purpose, non-porous wet solid particles of glass beads were contained in a vertical column and fluidized using air at ambient temperature. The fluidising air was virtually dry and obtained from a high-pressure compressor. An advanced imaging ECT sensor was used to provide dynamic information on the fluidized bed material distribution. The sensor was connected to a data acquisition unit and a computer. The air outlet temperature and its relative humidity were recorded using a temperature/humidity probe. Since the air condition at the inlet of the fluidization column was constant and completely independent of the bubbling bed operating conditions, only one probe was installed at the freeboard (air exit). The detailed experimental set-up is shown in Fig. 5.

6.1 Experimental procedure and materials

The fluidization was carried out in a cast acrylic column, 13.8 cm diameter and 150 cm high. The column was transparent, thus allowing for direct visual observation. A PVC perforated gas distributor with a total of 150 holes (~1.8% free area), was placed 24 cm above the column base. The upstream piping was fitted with pressure regulator, moisture trap, valve and three parallel rotameters. A one-step valve was connected before the moisture trap and was used as the upstream main flow controller. The particles used were ballotini (non-porous glass beads) with a mean diameter of 125 μm and a density of 2500 kg/m^3 (Geldart A/B mixture). The detailed physical properties of the particles are given in Table 1. Distilled water at ambient condition was used to wet the particles. A variable speed granule shaker was utilised to produce the final wetted mixture.

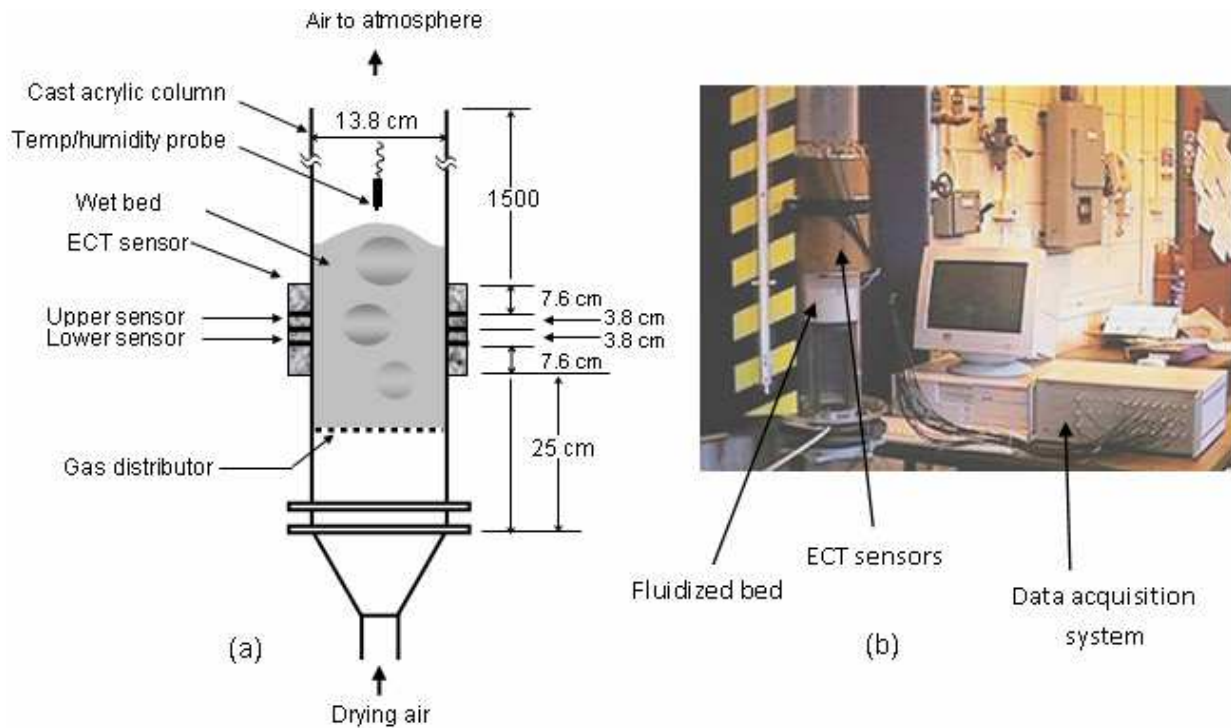


Fig. 5. Experimental set up (a) Schematic of the fluidized bed (b) A photograph of the installation

The Electrical Capacitance Tomography imaging system used (ECT from Process Tomography Limited, Manchester, UK), consisted of two adjacent sensor rings each containing 8 electrode of 3.8 cm length. All electrodes were connected to the computer through a data acquisition system. The PC was equipped with custom communication hardware and software that allow for online and off-line dynamic image display. The system is capable of taking cross-sectional images of the bed at two adjacent levels simultaneously at 100 frames per second. Further details about the ECT system used in this study and its application to fluidization analysis can be found in Makkawi et al. (2006) and Makkawi and Ocone (2007).

Geldart Group	A/B
Particle size range (μm)	50 - 180
Mean particle diameter (μm)	125
Particle density (kg/m^3)	2500
Sphericity	$\geq 80\%$
Pores	$< 0.02 \text{ nm}$
Material	Pure soda lime glass ballotini.
Chemical composition	$\text{SiO}_2=72\%$, $\text{Na}_2\text{O}=13\%$, $\text{CaO}=9\%$, $\text{MgO}=4\%$, $\text{Al}_2\text{O}_3=1\%$, K_2O & $\text{Fe}_2\text{O}_3=1\%$
Commercial name	Glass beads - type S, Art. 4500
Electric permittivity	~ 3.1

Table 1. Physical and chemical properties of the dry particles

The exit air quality was measured using a temperature and humidity probe (Type: Vaisala HMI 31, Vantaa, Finland, measuring range: 0-100% RH, -40-115 C°). The probe was hung by a connecting wire inside the fluidized bed freeboard approximately 10 cm above the maximum expanded bed height.

The experimental procedure employed was completely non-intrusive. The experiment commenced by weighting a total of 4.5 kg of a dry ballotini mixture and placing it in a granule shaker after being wetted by distilled water. The shaker was firmly clamped and operated continuously for at least 25 minutes to ensure an even distribution of water content. Distilled water was used to eliminate any possible interference with the ECT signal (ECT works for non-conducting materials only). The wetted particles were then loaded into the fluidization column. Prior to commencement of drying, the ECT sensor was calibrated for two extreme cases. This was carried out by sliding the ECT sensor up to the freeboard to calibrate for the empty bed case, and down to the static bed area to calibrate for the packed bed case. It should be mentioned that, because the water content was limited to a maximum of 45 ml (1% moisture on dry solid weight basis), the possible changes in the particle/air permittivity during the drying process would be negligible. Further details on the sensitivity of the ECT system to moisture content can be found in Chaplin and Pugsley (2005) and Chaplin et al., (2006). The wet bed material was fluidized at the required air flow rate. This was carefully adjusted to ensure the bed operation at the single bubble regime. The temperature and relative humidity were recorded at 2 minutes intervals. Simultaneously, and at the 5 minutes intervals, a segment of 60 seconds ECT data were recorded. At the same time, the expanded bed height during fluidization was obtained from visual observations. Finally, the drying rate was obtained from the measured air flow rate and temperature/humidity data at inlet and outlet using psychometric charts and mass balance calculations. The recorded ECT data were further processed off-line and loaded into in-house developed MATLAB algorithm to estimate the bubble characteristics.

The above described procedure was repeated for the three different operating conditions summarized in Table 2. To ensure data reproducibility, each operating condition was repeated three times, making a total of nine experiment tests.

Experimental unit	Operating conditions		
Fluidization column	Diameter = 13.8 cm, height = 150 cm, material: cast acrylic, equipped with a Perforated PVC plate of 150 holes, each of 2 mm dia.		
Dry particles	$d_p = 125 \mu\text{m}$, $\rho_p = 2500 \text{ kg/m}^3$, Material: glass		
Fluidization fluid	Air at ambient condition ($\sim 20^\circ \text{C}$)		
Static bed height	20 cm		
	Exp. 1	Exp. 2	Exp. 3
Fluidization velocity (m/s)	0.35	0.47	0.47
Initial water content (wt%)	1.0	1.0	0.5

Table 2. Summary of experimental operating conditions

6.2 Measurement of mass transfer coefficient

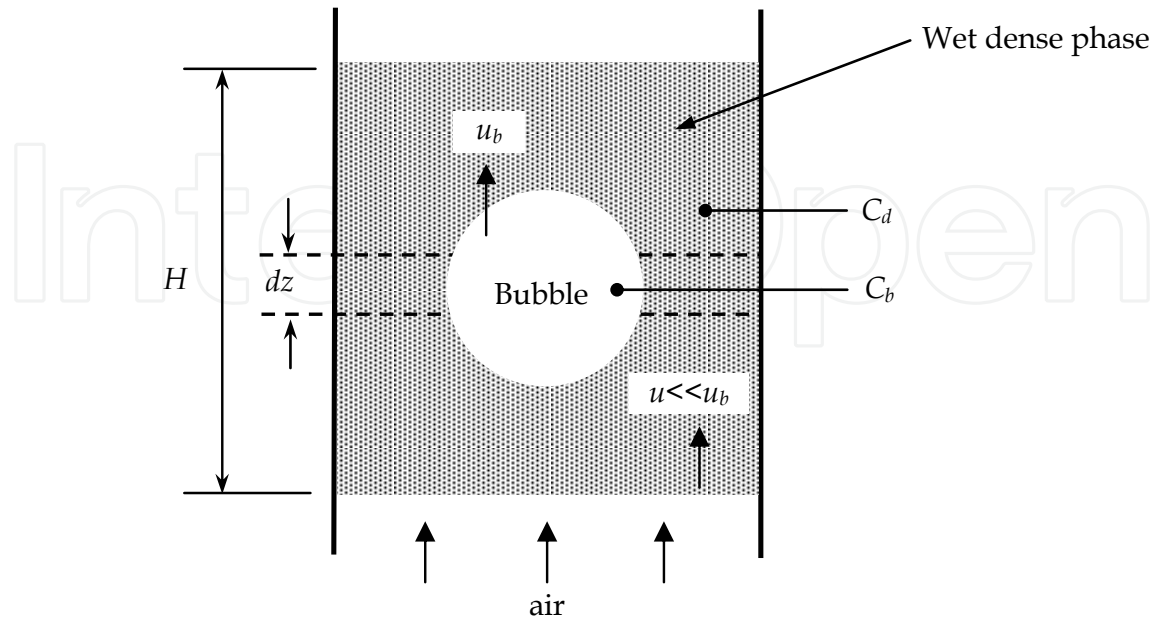


Fig. 6. Schematic representation of the method used in experimental calculation of the overall mass transfer coefficient

Considering a section of the bed as shown in Fig. 6, the overall mass transfer coefficient between the bubble phase and the surrounding dense phase, k_{db} , can be defined by the following rate equation:

$$-u_b \frac{dC_b}{dz} = \left(\frac{S_b}{V_b} \right) k_{db} (C_d - C_b) \quad (14)$$

where C_b is the water concentration in the bubble phase, C_d is the concentration in the surrounding dense phase, u_b , S_b and V_b are characteristic features of the bubble representing the rising velocity, the interphase area and the volume, respectively. For moisture-free inlet air, Eq. 14 is subject to the following boundary conditions:

$$C_b = (C_{in})_{air} = 0 \text{ at } z=0 \text{ and } C_b = (C_{out})_b \text{ at } z=H \quad (15)$$

where H is the expanded bed height. The bubble moisture content at the outlet $(C_{out})_b$ can be given by:

$$(C_{out})_b = \frac{(\text{drying rate})}{(\text{bubble mass flow rate})} = \frac{m_{air}(C_{out} - C_{in})_{air}}{m_b} \quad (16)$$

where m_{air} and m_b are the mass flow rate of the fluidising air and bubbles respectively. Because of the assumption that the bubbles rise much faster than the gas through the dense phase and the inlet air was virtually dry, Eq. 16 reduces to:

$$(C_{out})_b = (C_{out})_{air} \quad (17)$$

where $(C_{out})_{air}$ is obtained from the measured temperature and humidity at the bubbling bed surface.

For a spherical bubble, S_b/V_b ratio appearing in Eq. 14 reduces to $6/d_b$, where d_b is the bubble diameter. It should be mentioned that for a perforated distributor (such as the one used in this experiment), coalescence of bubbles mainly takes place at a few centimetres above the distributor, therefore, the entrance effects are neglected and the bubble characteristics are assumed independent of height (this was confirmed from the ECT images).

Finally, assuming that the water concentration in the dense phase is uniform and remains unchanged during the bubble rise ($C_d = w_{water}/w_{bed}$) and integrating Eq. 14 from $z=0$ to $z=H$, the mass transfer coefficient is obtained as follows:

$$k_{db} = -\left(\frac{d_b u_b}{6H}\right) \ln \left[\frac{C_d - (C_{out})_b}{C_d} \right] \quad (18)$$

where d_b and u_b are the bubble diameter and velocity respectively.

The experimental measurement of the overall mass transfer coefficient, k_{db} , as a function of the water concentration in the bed is shown in Fig. 7. The values of k_{db} are found to fall within the range of 0.0145-0.021 m/s. It is interesting to note that this range is close to the value one can obtain from the literature for the mass transfer coefficient from a free water surface to an adjacent slow moving ambient air stream (~ 0.015 m/s) (Saravacos and Z. Maroulis, 2001).

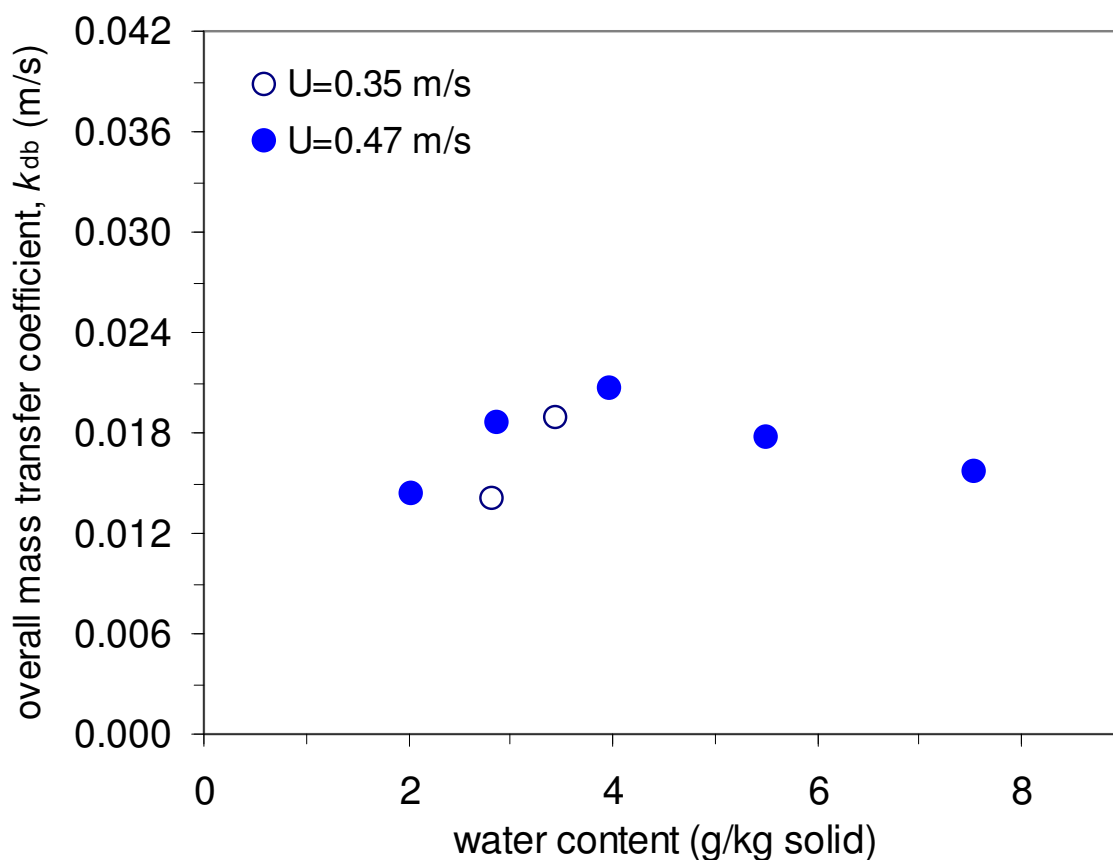


Fig. 7. Experimentally measured overall mass transfer coefficient

6.3 Measurement of bubble characteristics

Experimental determination of the overall mass transfer requires knowledge of the bubble diameter and velocity (see Eq. 18). Using the ECT, the diameter and velocity of the bubbles in a gas-solid fluidized bed can be obtained. The distinct lowering of the solid fraction when the bubble passes across the sensor area, as shown in Figs 11 and 12, allows for identification of the bubble events in a given time and space. The bubble velocity was then calculated from the delay time determined from a detailed analysis of the signal produced by the two adjacent sensors, such that:

$$u_b = \frac{\delta}{\Delta t_b} \quad (19)$$

where $\Delta t_b = t_{b2} - t_{b1}$, t_{b1} and t_{b2} represent the time when the bubble peak passes through the lower and upper level sensors respectively, and δ represents the distance between the centre of the two sensors, which is 3.8 cm. The method is demonstrated for a typical ECT data in Fig. 8.

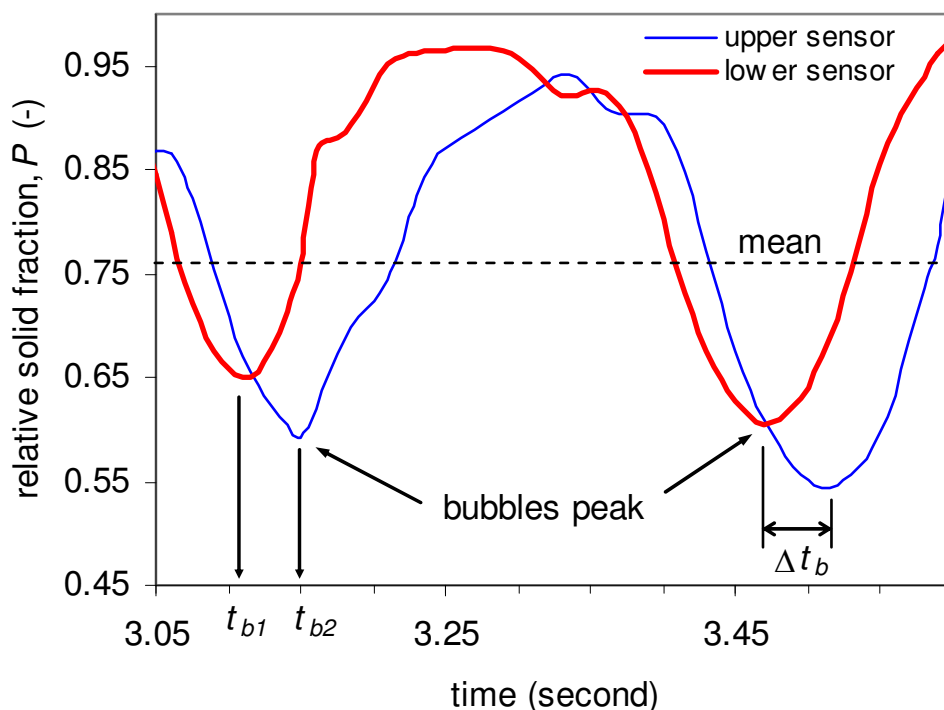


Fig. 8. Estimation of bubble velocity from ECT data

The bubble diameter was obtained from the ECT data of relative solid fraction at the moment of bubble peak across the sensor cross-section. From this, the bed voidage fraction (the fraction occupied by bubbles) was calculated as follows:

$$d_b = D\gamma \quad (20)$$

where $\gamma = (1 - P)$ is the bubble fraction, P is the relative solid fraction (i.e. packed bed: $P = 1$; empty bed: $P = 0$) and D is the bed/column diameter. This procedure is demonstrated for a typical ECT data in Fig.9. Further details on the application of twin-plane ECT for the measurements of bubble characteristics in a fluidized bed can be found in Makkawi and Wright (2004).

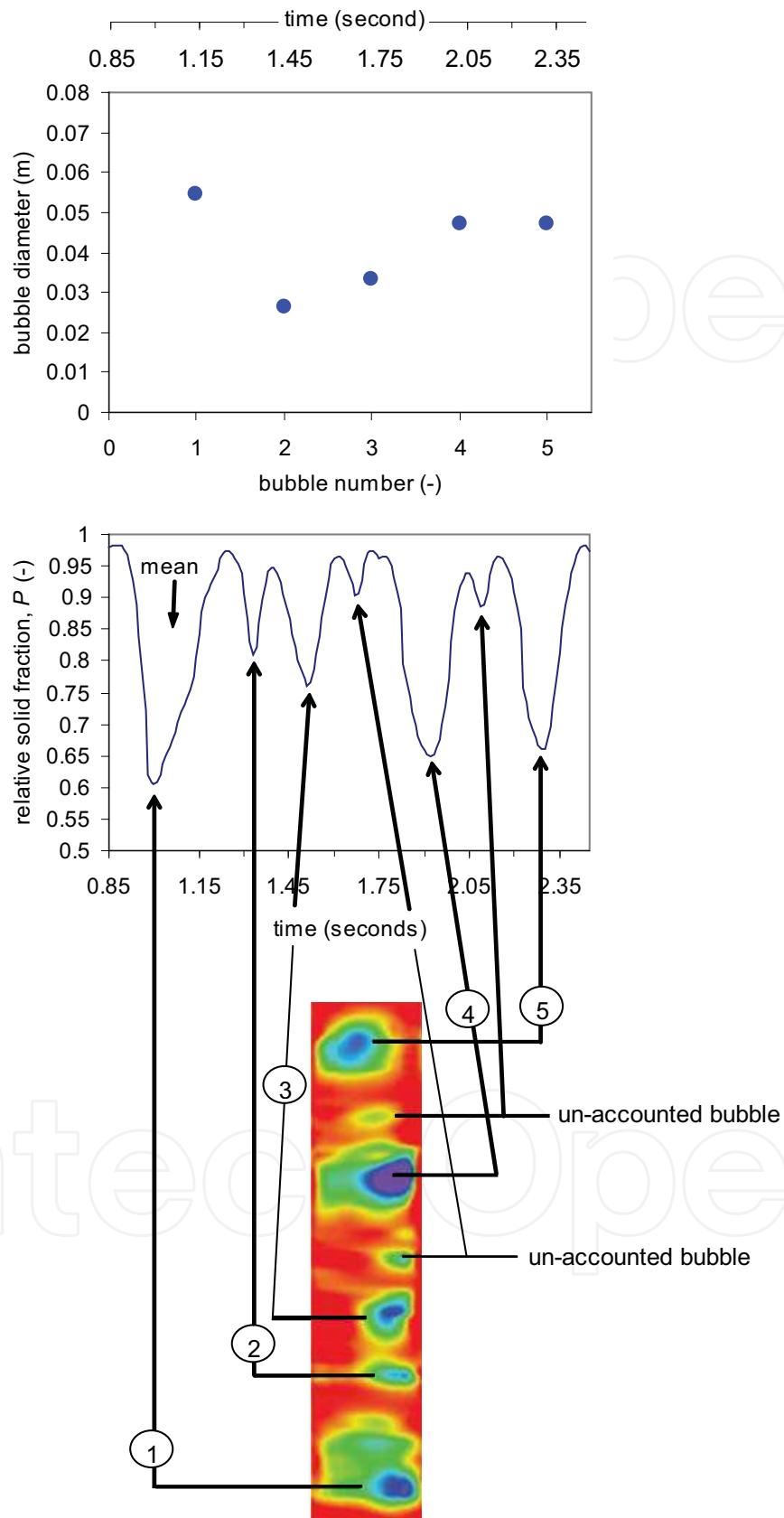


Fig. 9. Estimation of bubble diameter from ECT measurement (a) bubble diameter (b) ECT solid fraction (b) ECT slice images

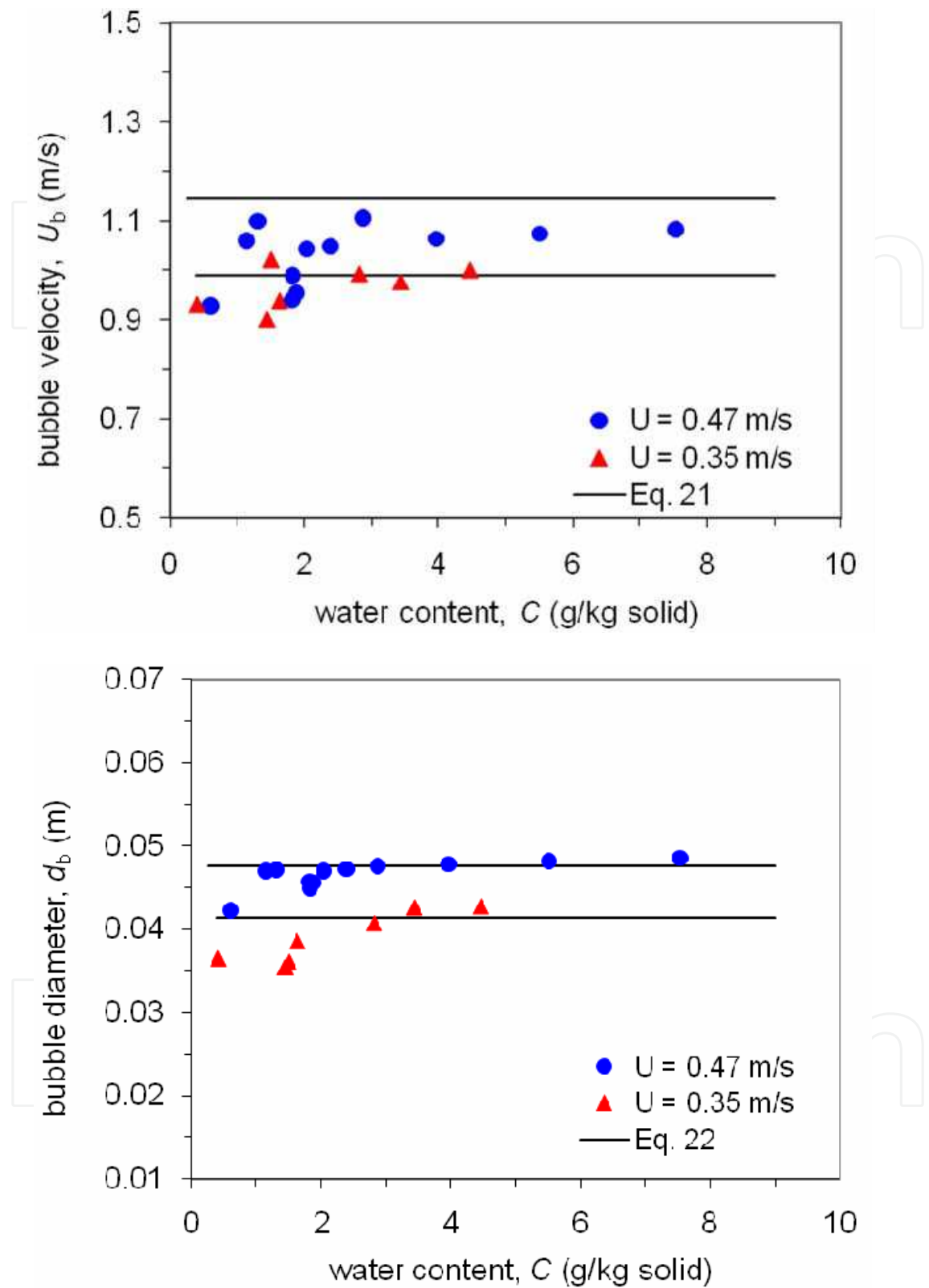


Fig. 10. Variation of the bubble velocity and bubble diameter during the drying process

Fig. 10 shows the measured bubble velocity and bubble diameter as a function of the water content in the bed. These measurements were taken at different time intervals during the drying process. Each data point represents the average over 60 seconds. Both parameters

vary slightly within a limited range. These hydrodynamic observations suggest that the bubble characteristics almost remain independent of the water content, at least within the range of operating conditions considered here. This is due to the fact that the initial water content in the bed was not significant enough to cause considerable hydrodynamic changes. Among the available correlations from the literature, the following equations have been found to provide good matches with the experimental measurements:

Bubble velocity:

$$u_b = \psi(U - U_{mf}) + \alpha \left[0.711(gd_b)^{0.5} \right] \quad (21)$$

This is a modified form of Davidson and Harrison [13] equation, where $\psi = 0.75$ and $\alpha = 3.2D_c^{1/3}$ are correction factors suggested by Werther(1991) [17] and Hillgardt and Werther(1986).

Bubble diameter:

$$d_b = 0.652 \left[D_o - \exp(-0.3z/D_c) \right] + \frac{0.347D_o}{n_o^{0.4}} \exp(-0.3z/D_c) \quad (22)$$

where

$$D_o = \left[\frac{\pi}{4D_c^2} (U - U_{mf}) \right]^{0.4} \quad (23)$$

U_{mf} used in Eqs 21 and 23 was given by:

$$U_{mf} = \frac{d_p^2 (\rho_p - \rho_g) g}{150\mu} \frac{\varepsilon_{mf}^3 \phi_p}{(1 - \varepsilon_{mf})} \quad (24)$$

For the operating condition given in Table 2, Eq. 24 gives $U_{mf} = 0.065$ m/s, which closely matches the measured value of 0.062 m/s. Despite the fact that Eqs. 21-24 were all originally developed for dry bed operations; they seem to provide a reasonable match with the experimental measurements made here under wet bed condition. This is not surprising, since the water content in the bed was relatively low as discussed above. The expanded bed height, used in the experimental estimation of the overall mass transfer coefficient (Eq. 18), is shown in Fig. 11. Limited increase in the bed expansion as the water is removed from the bed can be noticed.

6.4 Combined hydrodynamics and mass transfer coefficient model

In this analysis we assume that mass transfer occurs in two distinct regions: at the dense-cloud interface and at the cloud-bubble interface. The overall mass transfer may be dense-cloud controlled; cloud-bubble controlled or equally controlled by the two mechanisms depending on the operating conditions. The following theoretical formulations of these acting mechanisms are mainly based on the following assumptions:

- i. The fluidized bed operates at a single bubble regime.
- ii. The bubbles are spherically shaped.
- iii. The bubble rise velocity is fast ($u_b > 5U_{mf} / \varepsilon_{mf}$).

- iv. The bubbles size and velocity are independent of height above the distributor
- v. The contribution of particles presence within the bubble is negligible.
- vi. The contribution of the gas flow through the dense phase (emulsion gas) is assumed to be negligible.

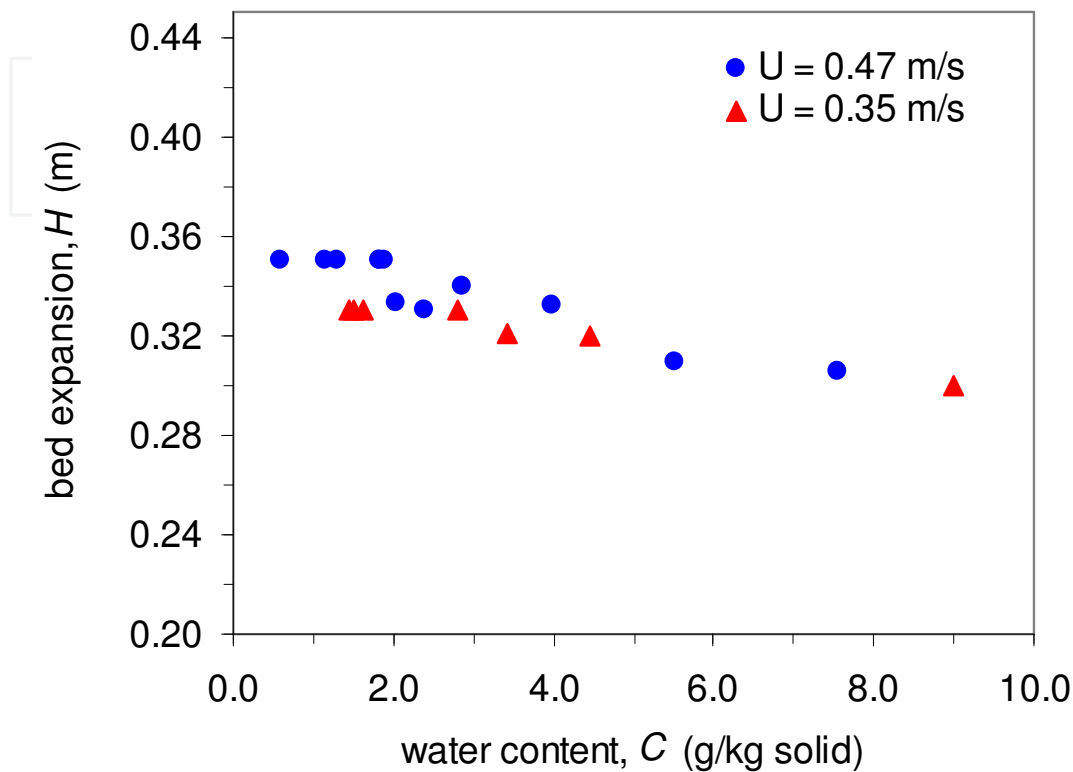


Fig. 11. Variation of expanded fluidized bed height during the drying process

As evident from the tomographic analysis of the bubble characteristics shown in Figs 2, 9 and 12, assumptions (i)-(v) are to a great extent a good representation of the actual bubbling behaviour considered here.

In this study, we assume the mass transfer at the bubble-cloud interface arises from two different contributions:

1. Convection contribution as a result of bubble throughflow, which consists of circulating gas between the bubble and the cloud, given by

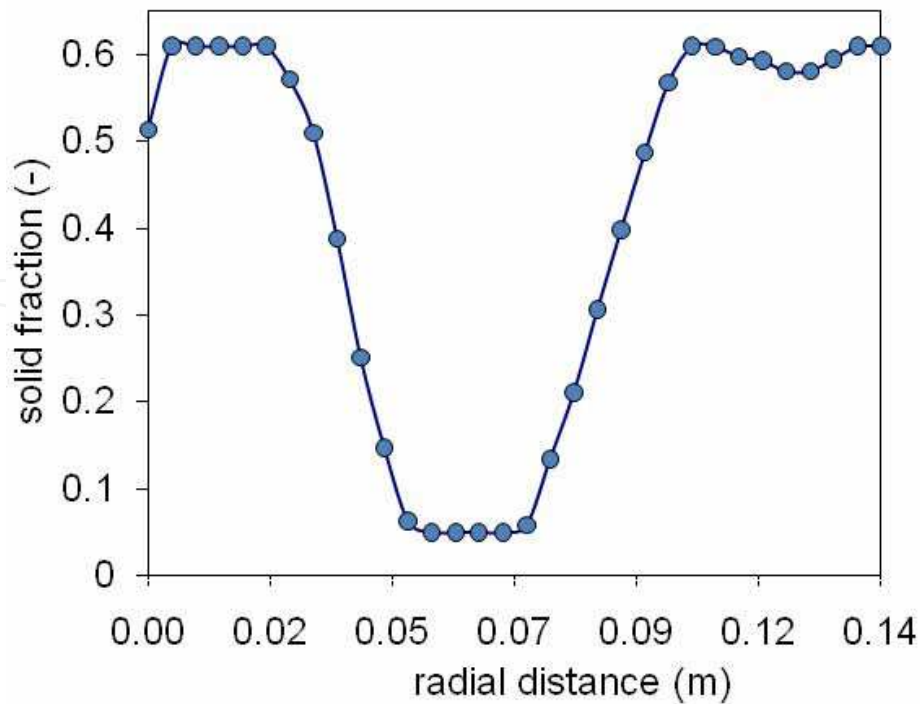
$$k_q = 0.25U_{mf} \quad (25)$$

2. Diffusion across a thin solid layer (cloud), given by

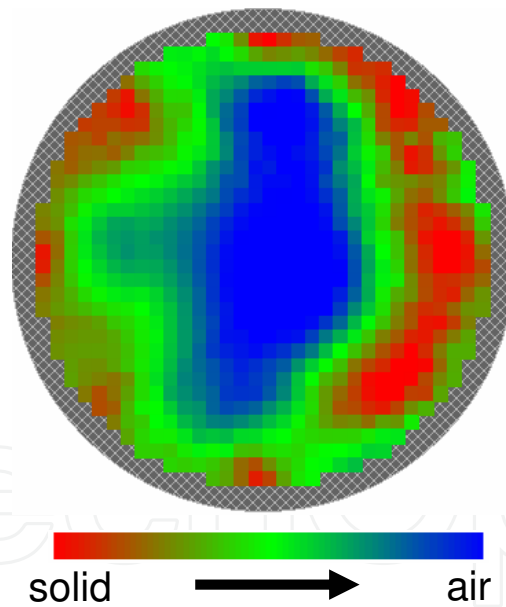
$$k'_{cb} = 0.975\mathcal{D}^{0.5} \left(\frac{g}{d_b} \right)^{0.25} \quad (26)$$

The addition of both acting mechanisms gives the total cloud-bubble mass transfer coefficient,

$$k_{cb} = 0.25U_{mf} + 0.975\mathcal{D}^{0.5} \left(\frac{g}{d_b} \right)^{0.25} \quad (27)$$



(a)



(b)

Fig. 12. Cross-sectional tomographic imaging during bubble passage across the sensor demonstrating negligible solid within the bubble core (a) radial solid concentration (b) contour of solid distribution

This suggest that the cloud-bubble interchange is indirectly proportional to the particle size (U_{mf} increases with increasing d_p) and inversely proportional to d_b . Note that the above equation reduces to the same formulation given earlier for the exchange coefficient (Eq. 5) after dividing by the bubble volume per unit area.

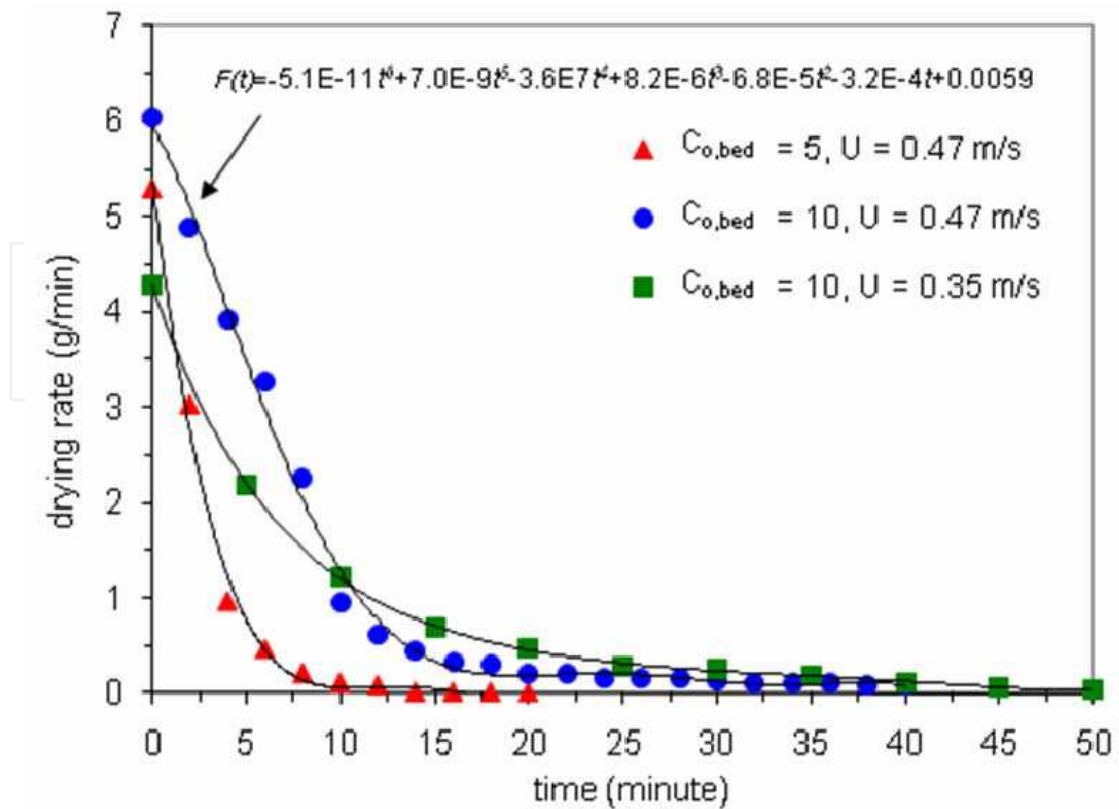


Fig. 13. Drying rate curves for the three conducted experiments

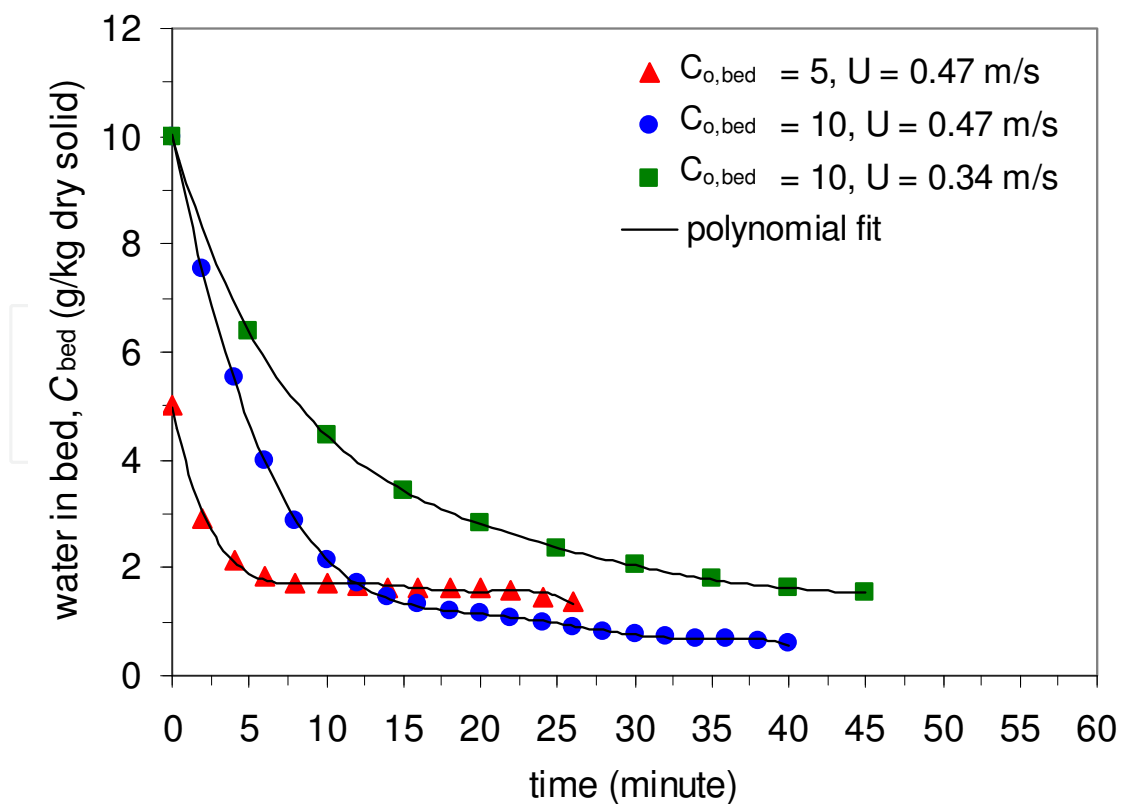


Fig. 14. Variation of water content during drying

The mass interchange coefficient across the dense-cloud boundary can be given by Higbie penetration mode (Eq. 10). For the special case discussed here, the tomographic images of the bubbles and its boundaries suggest that the cloud diameter (the outer ring in Fig. 2) is always within the range of 1.2-1.8 bubble diameters. Therefore, assuming that $d_c \sim 1.5d_b$, and after multiplying by bubble volume per unit area, the dense-cloud mass transfer coefficient can be given by:

$$k_{dc} = 0.92 \left(\frac{\mathcal{D} \varepsilon_{mf} u_b}{d_b} \right)^{0.5} \quad (28)$$

For an equally significant contribution from cloud-bubble and dense-cloud interchanges, Kunii and Levenspiel (1991) suggested adding both contributions in analogy to parallel resistances, such that the overall bed mass transfer coefficient (k_{db}) is given by:

$$\frac{1}{k_{db}} = \frac{1}{k_{dc}} + \frac{1}{k_{cb}} \quad (29)$$

Substituting Eq. 25 and 26 into Eq. 27 yields the overall mass transfer coefficient as follows:

$$k_{db} = \frac{A_1 B_1}{d_b^{0.5} (A_1 + B_1)} \quad (30)$$

where

$$A_1 = 0.975 \mathcal{D}^{0.5} (d_b g)^{0.25} + 0.25 U_{mf} d_b^{0.5} \quad (31)$$

$$B_1 = 0.92 (\mathcal{D} \varepsilon_{mf} u_b)^{0.5} \quad (32)$$

In this model, the bubble diameter and velocity are obtained from the correlations given in Eqs 21 and 22 respectively, and U_{mf} is given by Eq. 24.

6.5 Drying rate

The drying rate curves for the three experiments conducted are shown in Figure 13. The curve fitting is used to obtain the water content in the bed at various times. From this figure, it may be concluded that the drying time is directly proportional to the initial water content, and inversely proportional to the drying air flow rate. For instance, at an air velocity of 0.47 m/s, this time was reduced by half when reducing the initial water content from $C_{o,bed} = 10\%$ to $C_{o,bed} = 5\%$, while at the initial water content of $C_{o,bed} = 10$, this time was ~35% longer when reducing the air velocity from 0.47 m/s to 0.33 m/s. The water concentration in the bed as a function of the drying time is shown in Fig. 14. This was obtained from the integration of the drying curve function as given earlier in Eq. 13.

6.6 Comparison with literature data

Walker (1975) Sit and Grace (1978) measured the mass transfer coefficient in a two-dimensional fluidized bed. The technique employed involves the injection of ozone ozone-

rich bubble into an air-solid fluidized bed. Patel et al. (2003) reported numerical prediction of mass transfer coefficient in a single bubbling fluidized bed using a two fluid model based on kinetic theory of granular flow. Comparison between the above mentioned literature and the experimental data obtained in this study is shown in Fig. 15. Taking into consideration the differences in the experimental set-up and operating conditions, the agreement with our measurement appears satisfactory for the particle size considered in this study.

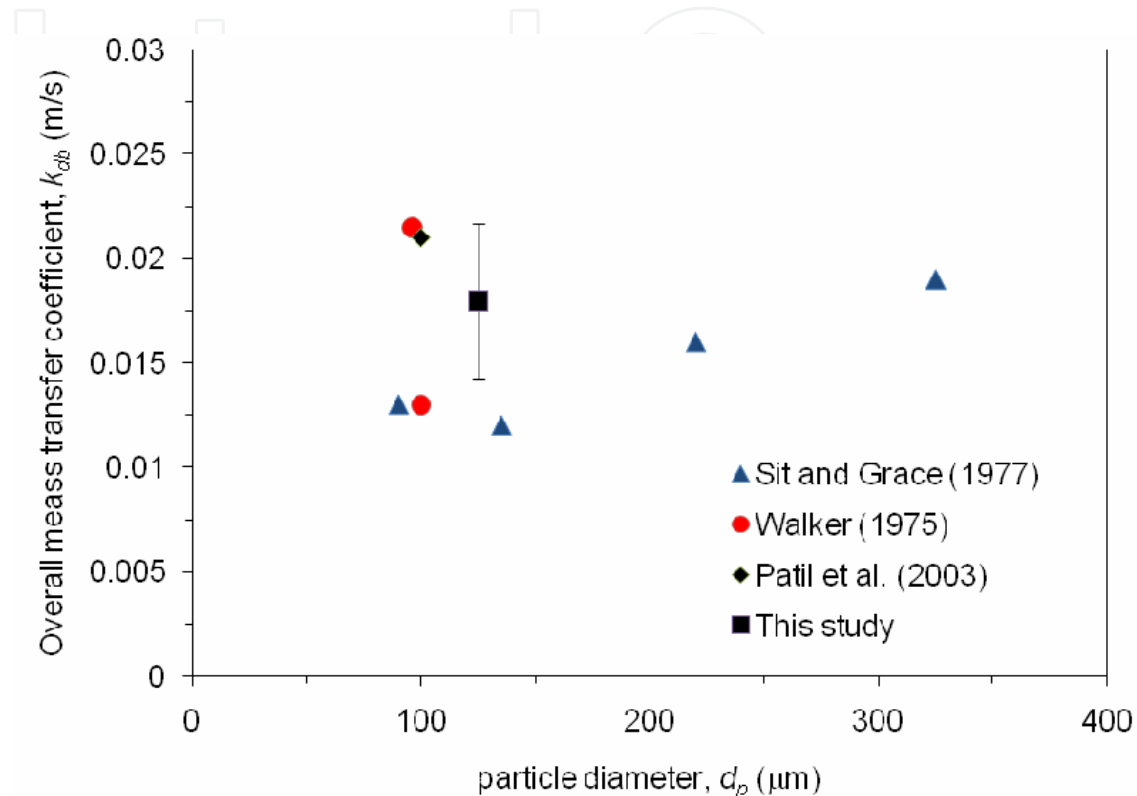


Fig. 15. Experimental overall mass transfer coefficient in comparison with other previously reported results

6.7 Comparison of experimental and theoretical prediction

Fig. 16 compares the measured mass transfer coefficient with the theoretical predictions obtained from the formulations given in section 6.4. The boundaries for the overall mass transfer coefficient are given by: (i) a model accounting for cloud-bubble and dense-bubble diffusion contribution as well as the bubble through flow convective contribution, giving the lower limit (Eq. 30) and (ii) a model accounting for the cloud-bubble contribution, giving the upper limit (Eq. 27). The results also suggest that, within the operating conditions considered here, the drying may well be represented by a purely diffusional model, controlled by either the resistance residing at the dens-cloud interface, or the cloud-bubble interface.

Finally, Table 3 shows the numerical values of the various mass transfer contributions obtained from Eqs 25-32. It is shown that the estimated diffusional resistances, as well as the contribution from the bubble throughflow, are all of the same order of magnitude. Previously, Geldart (1968) argued that the bubble throughflow is not important for small particles and may be neglected. According to our analysis, this may well be the case here. However, generalization of this conclusion should be treated with caution especially when dealing with larger particles.

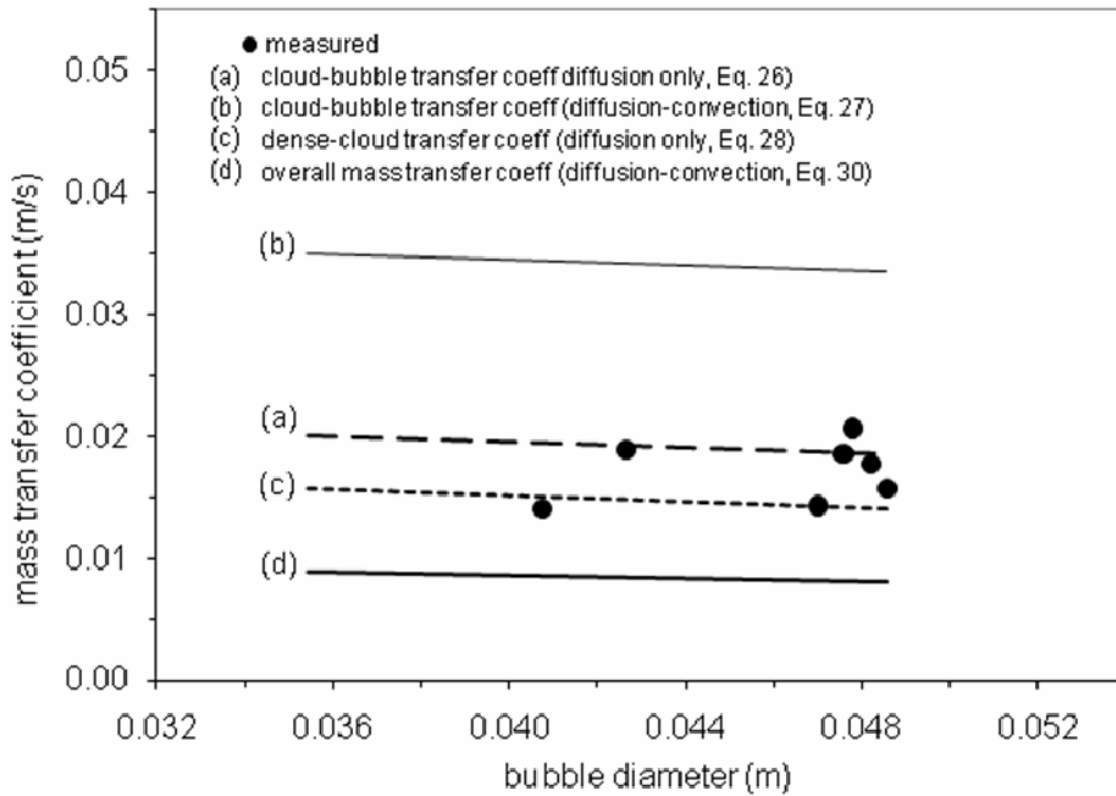


Fig. 16. Comparison between experimental measurement and various theoretical models for mass transfer coefficients

Experimental				Theoretical		
Gas velocity	bubble characteristics		Overall mass transfer coeff.	Dense-cloud interchange (diffusion only)	Cloud-bubble interchange (diffusion only)	Bubble throughflow
	U (m/s)	d_b (m)		u_b (m/s)	k_{dc} (m/s)- Eq. 28	k_{cb} (m/s)- Eq. 27
0.35	0.04	0.99	0.0145	0.0178	0.0194	0.015

Table 3. The measured overall mass transfer coefficient for one selected operating condition in comparison to the theoretical predictions of various contributions.

6.8 Conclusion

Mass transfer coefficient in a bubbling fluidized bed dryer has been experimentally determined. This work is the first to utilise an ECT system for this purpose. The ECT allowed for quantification of the bubble diameter and velocity, as well as providing new insight into the bubble-cloud-dense boundaries.

The measured overall mass transfer coefficient was found to be in the range of 0.045-0.021 m²/s. A simple hydrodynamic and mass transfer model, based on the available correlations

was used to predict the mass transfer coefficient in a bubbling fluidized bed. Despite the complexity of the process, and the number of assumption employed in this analysis, the model based on pure diffusional mass transfer seems to provide satisfactory agreement with the experimental measurements.

This work set the scene for future experimental investigations to obtain a generalised correlation for the mass transfer coefficient in fluidized bed dryer, particularly that utilizes the ECT or other similar imaging techniques. Such a correlation is of vital importance for improved fluidized bed dryer design and operation in its widest application. A comprehensive experimental program, covering a wider range of operating conditions (particle size, gas velocity, water content, porous/non-porous particles) is recommended.

7. Nomenclature

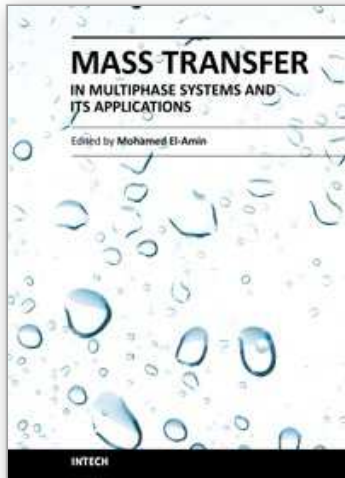
A	[m ²]	column/bed cross-sectional area
A_1, B_1	[m ^{1.5} s ⁻¹]	parameters defined in Eqs. 15, 16 respectively
C_d, C_b	[-]	water concentration in the dense and bubble phases respectively, kg/kg
d, D	[m]	diameter
$\mathcal{D}, \mathcal{D}_e$	[m ² s ⁻¹]	molecular and effective diffusivity respectively
g	[ms ⁻²]	gravity acceleration constant
H	[m]	expanded bed height
k_{db}	[ms ⁻¹]	overall mass transfer coefficient (between dense and bubble phases)
k_{cb}	[ms ⁻¹]	mass transfer coefficient between cloud and bubble phases
k_{dc}	[ms ⁻¹]	mass transfer coefficient between dense and cloud phases
m	[kgs ⁻¹]	mass flow rate
P	[-]	relative solid fraction
P	[-]	relative solid fraction
U	[ms ⁻¹]	superficial gas velocity
u	[ms ⁻¹]	velocity
V	[(m ³)	volume
w	[g]	bed water content
z	[m]	axial coordinate
Greek symbols		
ε	[-]	bed voidage
γ	[-]	bubble fraction
ρ	[kg.m ⁻³]	density
δ	[m]	distance between the centre of the two ECT sensors
φ_p	[-]	particle sphericity
Subscripts		
b		bubble
c		cloud
d		dense
mf		minimum fluidization
p		particle

8. References

- Agarwal, P.K. (1987). The residence phase of active particles in fluidized beds of smaller inert particles. *Chemical Engineering Science* 42, 2481-2483
- Chaplin G. and Pugsley, T. (2005). Application of electrical capacitance tomography to the fluidized bed drying of pharmaceutical granule. *Chemical Engineering Science* 60, 7022.
- Chaplin, G., pugsley, T., van der, L., Kantzas, A., Winter's, C. (2005). The dynamic calibration of an electrical capacitance tomography sensor applied to the fluidised bed drying of pharmaceutical granule, *Measurement Science and Technology* 16, 281.
- Chiba, T. and Kobayashi, H. (1970). *Chemical Engineering Science* 25,1375.
- Ciesielczyk, W. and Iwanowski, J. (2006). Analysis of Fluidized Bed Drying Kinetics on the Basis of Interphase Mass Transfer Coefficient, *Drying Technology* 24, 1153-1157.
- Davidson, J. and Harrison, D. (1963). *Fluidized Particles*, Cambridge University Press, Cambridge, England.
- Frossling, N. (1938). The evaporation of falling drops. *Gerlands Beitrage zur Geophysik* 52, 170-216 (in German).
- Geldart, D. (1986). *Gas Fluidization Technology*, John Wiley and Sons, Chichester, UK.
- Higbie, R., in *Fluidization Engineering* (1991), Second edition (Eds: D. Kunii and O. Levenspiel), Butterworth-Heinemann, Boston, USA.
- Hillgardt, K. and Werther, J. (1986). Local bubble gas-holdup and expansion of gas/solid fluidized beds. *Ger. Chem. Eng.*, 9, 215-221. *German Chemical Engineering* 9, 215.
- Keey, R. B., Introduction to industrial drying operations (1978), Pergamon Press Ltd., Headington Hall, Oxford, England.
- Kerkhof, P. J. A. M. (2000). Some modeling aspects of (batch) fluid-bed drying of life-science products. *Chemical Engineering and Processing*, 39, 69.
- Kunii, D. and Levenspiel, O. (1991). *Fluidization Engineering*. Second edition, Butterworth-Heinemann, Boston.
- Makkawi, Y. and Ocone, R. (2007). Integration of ECT measurements with hydrodynamic modelling of conventional gas-solid bubbling bed. *Chemical Engineering Science*. 4304-4315.
- Makkawi, Y., Wright, P. C., Ocone, R. (2006). The effect of friction and inter-particle cohesive forces on the hydrodynamics of gas-solid flow: a comparative analysis of theoretical predictions and experiments. *Powder Technology* 163. 69-79.
- Makkawi, Y. and Wright, P. C. (2004). Electrical Capacitance Tomography for conventional fluidized bed measurements- remarks on the measuring technique. *Powder Technology* 148. 142-157.
- Mori, S. and Wen, C. Y. (1975). Estimation of bubble diameter in gaseous fluidized beds. *AIChE Journal*, 21: 109-115.
- Murray, J. D. (1965). On the mathematics of fluidization Part 2. Steady motion of fully developed bubbles. *Journal of Fluid Mechanics*, 22, 57-80.
- Patil, D. J., van Sint Annaland, M., Kuipers, J. A. M. (2003). Gas Dispersion and Bubble-to-Emulsion Phase Mass Exchange in a Gas-Solid Bubbling Fluidized Bed: A Computational and Experimental Study, *International Journal of Chemical Engineering*, 1-20.
- Saravacos G. and Maroulis, Z. (2001). *Transport properties of foods*, CRC Press.

- Scala, F. (2007). Mass transfer around freely moving active particles in the dense phase of a gas fluidized bed of inert particles, *Chemical Engineering Science*, 62(16), 4159-4176
Chemical Engineering Science 62, 4159.
- Sit, S. P. and Grace, J. R. (1978). Interphase mass transfer in aggregative fluidized beds. *Chemical Engineering Science*, 33, 1115.
- Toomey, R.D. and Johnstone, H.F., Gaseous Fluidization of Solid Particles. *Chem. Eng Prog.* 48, 220-226, 1952
- Walker, B. V. (1975). *Transaction Institute of Chemical Engineers*, 53, 225.
- Werther, J., in *Fluidization Engineering* (1991), Second edition (Eds: D. Kunii and O. Levenspiel), Butterworth-Heinemann, Boston, USA

IntechOpen



Mass Transfer in Multiphase Systems and its Applications

Edited by Prof. Mohamed El-Amin

ISBN 978-953-307-215-9

Hard cover, 780 pages

Publisher InTech

Published online 11, February, 2011

Published in print edition February, 2011

This book covers a number of developing topics in mass transfer processes in multiphase systems for a variety of applications. The book effectively blends theoretical, numerical, modeling and experimental aspects of mass transfer in multiphase systems that are usually encountered in many research areas such as chemical, reactor, environmental and petroleum engineering. From biological and chemical reactors to paper and wood industry and all the way to thin film, the 31 chapters of this book serve as an important reference for any researcher or engineer working in the field of mass transfer and related topics.

How to reference

In order to correctly reference this scholarly work, feel free to copy and paste the following:

Yassir T. Makkawi and Raffaella Ocone (2011). Mass Transfer in Fluidized Bed Drying of Moist Particulate, Mass Transfer in Multiphase Systems and its Applications, Prof. Mohamed El-Amin (Ed.), ISBN: 978-953-307-215-9, InTech, Available from: <http://www.intechopen.com/books/mass-transfer-in-multiphase-systems-and-its-applications/mass-transfer-in-fluidized-bed-drying-of-moist-particulate>

INTECH
open science | open minds

InTech Europe

University Campus STeP Ri
Slavka Krautzeka 83/A
51000 Rijeka, Croatia
Phone: +385 (51) 770 447
Fax: +385 (51) 686 166
www.intechopen.com

InTech China

Unit 405, Office Block, Hotel Equatorial Shanghai
No.65, Yan An Road (West), Shanghai, 200040, China
中国上海市延安西路65号上海国际贵都大饭店办公楼405单元
Phone: +86-21-62489820
Fax: +86-21-62489821

© 2011 The Author(s). Licensee IntechOpen. This chapter is distributed under the terms of the [Creative Commons Attribution-NonCommercial-ShareAlike-3.0 License](#), which permits use, distribution and reproduction for non-commercial purposes, provided the original is properly cited and derivative works building on this content are distributed under the same license.

IntechOpen

IntechOpen